HALF-INTEGER RESONANCE CROSSING AND SPACE-CHARGE LIMIT *

A.V. Fedotov
BNL, Upton, NY 11973, USA
I. Hofmann
GSI, Planckstr 1, 64291 Darmstadt, Germany

Abstract

We study the influence of space charge on the crossing of the second-order resonance and the associated space-charge limit in high-intensity rings. Two-dimensional simulation studies are compared and found to agree with the envelope models in the finding of an increased intensity limit due to the coherent frequency shift. We also discuss application of this effect to bunched beams and multi-turn injection painting, and the effect of high-order resonances and issues of the envelope instability.

1 INTRODUCTION

A correct treatment of resonance crossing in the presence of space charge must take into account the coherent behavior of the beam [1]. Recently, we applied coherent resonance theory to the space-charge limit studies in the SNS [2]. First, we confirmed collective resonance response of an unbunched beam for various beam distributions. We then extended our studies to a bunched beam as well as to the process of beam accumulation.

In general, the coherent resonance condition has the form:

$$n = \Omega_m \equiv m\nu_0 - \Delta\Omega_m, \qquad (1)$$

where Ω_m is the frequency of the mth-order coherent beam mode, $\Delta\Omega_m$ is the coherent space-charge tune shift of the mth-order mode from its zero-current value ($m\nu_0$), and n stands for the error Fourier harmonic. In this paper we consider the $m = 2$ case which is associated with the space charge limit imposed by the half-integer resonance.

2 IMPERFECTION RESONANCE

2.1 Coherent space-charge limit

We start with exact numerical solutions of the envelope equations. First, we consider the 1/2 resonance near the unsplit-tune working point $\nu_{0,x,y} = 4.6$. We assume equal emittances in x and y and solve the envelope equations with error Fourier harmonics of $1 \cdot 10^{-3}$ units (relative to the unperturbed focusing constant), driving the $n = 9$ harmonic. The maximum envelope excursion grows with increasing beam intensity, which brings the coherent mode frequency closer to the resonance. Figure 1 shows the maximum envelopes for this case as the function of depressed incoherent tune $\nu_{x,y}$ for both the symmetric and anti-symmetric errors. The envelope increases noticeably only with the coherent frequency crossing the integer, which occurs at $\nu_{x,y} = 4.467$ (beam intensity equal to $\frac{4}{3}\Delta\nu_{inc}$) for the out-of-phase mode, and at $\nu_{x,y} = 4.4$ (beam intensity equal to $2\Delta\nu_{inc}$) for the in-phase mode. Due to the dependence of the envelope eigenfrequency on amplitude the maximum growth happens for higher beam intensities at $\nu_{x,y} = 4.44$ for the out-of-phase and $\nu_{x,y} = 4.37$ for the in-phase mode. A zero-current envelope response to this $1/2$ resonance is obtained by varying the working point $\nu_{0,x,y}$.

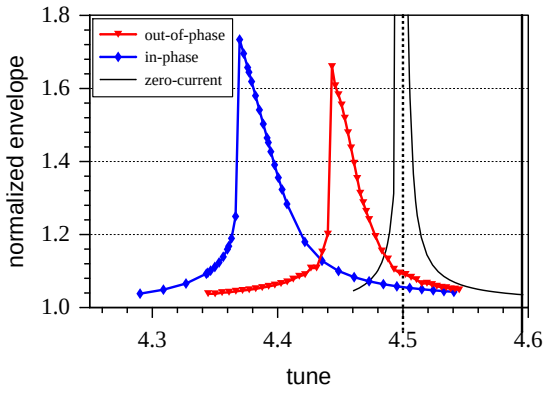

Figure 1: Response curves for the unsplit-tune working point (numerical solution of envelope equations).

The size of the maximum envelope excursion, as well as the width of the response curve, is a function of the strength of the imperfection resonance. Figure 2 shows the maximum y-envelopes for $(\nu_{0x}, \nu_{0y}) = (.45, 4.6)$ and three different magnitudes of error. The intensity parameter $I \equiv \Delta\nu_{sc}/\Delta\nu_{inc}$ (abscissa) is expressed as space-charge tune shift normalized to the distance from the bare tune to the half-integer ($\Delta\nu_{inc}$). The strongly asymmetric shape of the envelope response curves is a result of the nonlinear nature of the envelope equation, in particular the increase of envelope frequency with amplitude.

We now proceed to the realistic SNS lattice with the working point at $(\nu_{0x}, \nu_{0y}) = (6.45, 4.6)$. The gradient error is introduced in a single quadrupole with the normalized strength of an error $\Delta k = 2.5 \cdot 10^{-3}$ units. Simulations were done using the Particle-In-Cell (PIC) code ORBIT [3]. The results of simulations are presented in Fig. 3, which confirm the envelope response expected based on the envelope equations (Fig. 2). In Figs. 3-4, the maximum beam envelope for each intensity is plotted with blue

* Work supported by the US Department of Energy

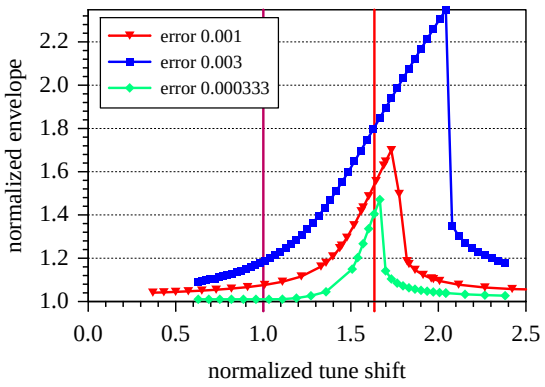

Figure 2: Response curves for various strengths of resonance driving error (solution of envelope equation). Incoherent space-charge limit corresponds to $I = 1$, while the coherent resonance condition in this case corresponds to $I = 1.635$.

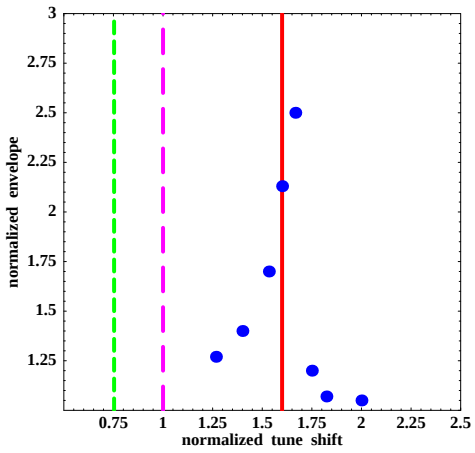

Figure 3: Response curve for the split-tune working point (PIC simulation, WB distribution, SNS lattice).

dots, the green (short dash) vertical line indicates the incoherent space-charge limit for a WB beam, the pink (long dash) line - the incoherent limit for uniform density beam, while red (solid) line - the coherent resonance condition [2]. These features of an envelope response were recently demonstrated for the LANL PSR [4] and the FNAL booster [5]. An important feature of coherent non-linear resonant response is different beam behavior depending on whether the resonance is crossed in the direction of increasing or decreasing space-charge effect. Recently, an experimental study of this effect was performed by Uesugi et al. [6].

3 STRUCTURE RESONANCE

One of the SNS working points $(\nu_{0x}, \nu_{0y}) = (6.23, 6.20)$ lies very close to the half-integer structure resonance with harmonic $n = 1$. It is thus extremely important to understand associated intensity limitation.

3.1 *Unbunched beams*

Simulations are done without errors so that only the lattice harmonics are present, with $n = 12$ being the structure harmonic due the SNS superperiodicity of 4. A single-particle dynamics approach would not allow the incoherent tune to approach an integer because of beam envelope beating, starting at intensities for which the incoherent tunes are still well above the integer (similar to the zero-current envelope response in Fig. 1) due to the finite bandwidth of the resonance. The space-charge limit for this working point corresponds to $4\Delta\nu_{inc}/3$ ($b = a$), but the beam envelope response to this coherent 1/2 resonance starts at lower intensities, similar to the response curves in Fig. 2. Simulations with both uniform and non-uniform distributions [2] confirmed the resonance response corresponding to coherent resonance intensities. An example of the response diagram is shown in Fig. 4.

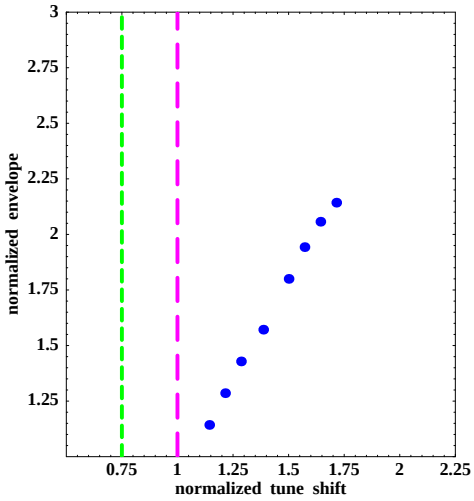

Figure 4: Response curve near the structure resonance (PIC simulations, WB distribution, SNS lattice).

3.2 *Bunched beams and multi-turn injection*

In the SNS, the full injection process takes about one synchrotron oscillation. It thus seems reasonable to expect that the impact of synchrotron motion will not be important. Simulations are performed with 1052-turn injection for a beam with momentum spread of $dp/p = 0.7\%$. The tune foot-prints of a final full intensity beam are plotted at the end of accumulation process. Figure 5 shows the foot-prints for three beam intensities: $N = 2 \cdot 10^{14}$ protons (red color), $N = 3 \cdot 10^{14}$ (pink color), $N = 4 \cdot 10^{14}$ (green color). Note that a dp/p spread was present in the simulation but its effect on the tune spread was excluded from the pictorial representation. A modification of the space-charge foot-print by the dp/p spread is discussed elsewhere [7]. For example, the combined tune spread (space charge and dp/p) extends down to the incoherent tune of 6.0 for

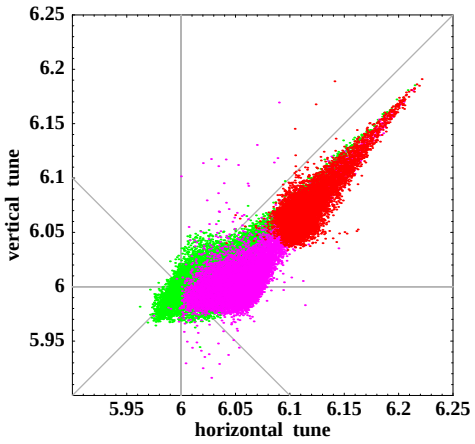

Figure 5: Tune footprints at the end of accumulation for three intensities of the beam.

the first case of $N = 2 \cdot 10^{14}$. The time evolution of the vertical rms emittances, corresponding to Fig. 5, is shown in Fig. 6. No resonant effect is observed until the beam gets into the bandwidth of the coherent resonance [2].

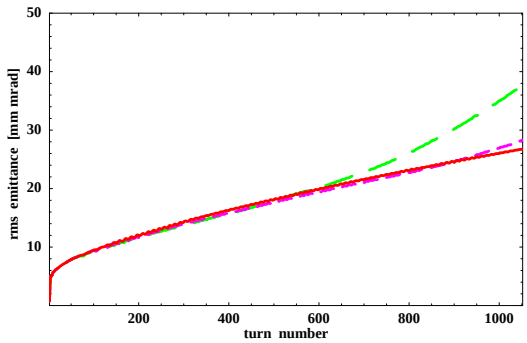

Figure 6: Vertical rms emittance during multiturn injection process for three intensities of the beam.

4 HIGH-ORDER RESONANCES

The coherent resonance condition for the high-order resonances is very close to the incoherent one. In some cases, the space-charge limit may be restricted by these high-order resonances. This, for example, is true when one has a split-tune working point with weak space charge coupling, as in the case of $(6.3, 5.8)$ of the SNS. As a result, the beam responds first to a fourth-order coherent sum resonance driven by the fringe fields with strong intensity limitation. On the other hand, for the $(6.23, 6.20)$ working point with strong space-charge coupling it was found that the space-charge limit is not significantly altered by the presence of the high-order resonance of realistic strength, which allows the beam intensity to increase slightly beyond $N = 2 \cdot 10^{14}$ for this working point [8]. The tolerable intensity limits is determined by allowed beam losses at restricting acceptance.

5 ENVELOPE INSTABILITY

The envelope instability occurs if the zero-current phase advance per focusing cell is above a quarter-integer, i.e. for $\sigma_0 > 90^0$. Space charge then leads to an extended stop-band starting slightly below $\sigma \Theta 9\ ^0$. Several cases of the envelope instability were explored [2]: 1) "superstructure" resonance, which is a direct analogy with the envelope instability in the transport channel [9], 2) envelope instability driven by the imperfection errors near the quarter-integer tunes, 3) envelope instability driven by the imperfection errors near the 1/2 tunes. In these studies we have used the KVXYG [10] code, which matches KV-envelopes and determines the eigenvalues (growth factors) of envelope perturbations. For example, for the case of the envelope instability near the 1/4 tunes we concluded that the imperfection driven envelope instability for working points above the fractional tune of 0.25 (likewise 0.75) is ignorable [2].

6 SUMMARY

Application of the coherent resonance condition both to the imperfection and structure resonances is discussed. We explore the applicability of such an effect to the SNS bunched beam and multi-turn injection process. In addition, we address the issue of the envelope instability in a circular machine.

7 ACKNOWLEDGMENTS

We are indebted to J. Holmes, R.L. Gluckstern and A. Burov for extensive useful discussions. We are also grateful to M. Blaskiewicz, Y.Y. Lee, Y. Papaphilippou, G. Parzen, J. Struckmeier and J. Wei for useful comments and discussions in the course of these studies.

8 REFERENCES

[1] L. Smith, Conf. on High Energy Acc. (Dubna, Russia, 1963), p. 1232; F. Sacherer, Lawrence Rad. Lab Report UCRL-18454 (Ph.D. thesis, 1968); I. Hofmann and K. Beckert, IEEE Trans. Nucl. Sci. NS-32 (PAC'85), p. 2264; S. Machida, Nucl. Inst. Meth. A309 (1991), p. 43; R. Baartman, AIP Conf. Proc. 448, (Ny, 1998), p. 56 and references therein.

[2] A.V. Fedotov and I. Hofmann, Phys. Rev. ST Accel. Beams, V 5, 024202 (2002).

[3] J. Galambos et al., ORBIT's User's Manual, SNS/ORNL/AP Technical Note 011 (1999).

[4] J. Holmes et al., Proc. of PAC'01 (Chicago), p. 3188 and references therein.

[5] M. D'yachkov et al., Proc. of PAC'01 (Chicago), p. 267.

[6] T. Uesugi et al., Proc. of EPAC'00 (Vienna), p. 1333 ; also T. Uesugi, Ph.D. dissertation (2000).

[7] A.V. Fedotov et al., Proc. of PAC'01 (Chicago), p. 2848.

[8] A.V. Fedotov (unpublished).

[9] I. Hofmann et al., Part. Accel., V 13, p. 145 (1983).

[10] J. Struckmeier and M. Reiser, Part. Accel. 14, p. 227 (1984).